Intuitive Assistive Robotic Manipulator (I-ARM)

A Final Year Project Report

Presented to

SCHOOL OF MECHANICAL & MANUFACTURING ENGINEERING

Department of Mechanical Engineering

NUST

ISLAMABAD, PAKISTAN

In Partial Fulfillment

of the Requirements for the Degree of

Bachelors of Mechanical Engineering

by

Saad Bin Saeed

Muhammad Saad Zafar

Syed Hadi Raza Zaidi

Muhib Ur Rehman Farooqui

June 2024

EXAMINATION COMMITTEE

We hereby recommend that the final year project report prepared under our supervision by:

Saad Bin Saeed	331486.
Muhammad Saad Zafar	332264.
Syed Hadi Raza Zaidi	336521
Muhib Ur Rehman Farooqui	338565

Titled: "Intuitive Assistive Robotic Manipulator" be accepted in partial fulfillment of the requirements for the award of Bachelors of Mechanical Engineering degree with grade ___

Supervisor: Dr. Asim Waris, Assistant Professor
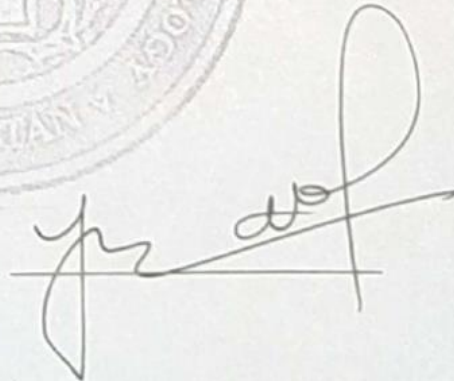HoD Biomedical Engineering, SMME

Dated: 12/6/2024

_____
(Head of Department)

12/06/2024
(Date)

COUNTERSIGNED

Dated: 12/6/24

i

<u>ABSTRACT</u>

This project presents the design and fabrication of an intuitive robotic manipulator tailored for assistive use by individuals with but not limited to upper limb disabilities. This initiative aims to enhance user quality of life by enabling them to perform tasks that might otherwise be challenging or impossible, promoting autonomy and accessibility. The manipulator leverages an EMG and IMU based control system for intuitive operation, wirelessly controlling the robot through a wearable device. Its versatility encompasses functions like grasping objects and executing various movements. The project incorporates a multi-pronged approach, emphasizing mechanical design, electronic integration, and user-centric programming. Safety, reliability, and user-friendliness are paramount considerations. A key driver is to reduce the cost of assistive technology. This necessitates a cost-effective approach, employing 3D printing (FDM process with PLA) for select components and readily available electromechanical actuators. The manipulator boasts three degrees of freedom with revolute joints and an adaptive fin gripper end effector.

ACKNOWLEDGMENTS

ORIGINALITY REPORT

TABLE OF CONTENTS

LIST OF FIGURES

LIST OF TABLES

ABBREVIATIONS

PLA	Polylactic Acid
PETG	Polyethylene Terephthalate (glycol)
ABS	Acrylonitrile Butadiene Styrene
EMG	Electro Myography
EEG	Electroencephalography
IMU	Inertial Measurement Unit
DH Parameters	Denavit-Hartenberg parameters

CHAPTER 1: INTRODUCTION

ASSISTIVE TECHNOLOGY, CHARTING NEW FRONTIERS IN REHABILITATION:

Per US sources, nearly 5.4 million people suffer from upper limb deformities and paralysis. These conditions include but are not limited to spinal muscular atrophy, acheiria, aphalangia, amyotrophic lateral sclerosis, congenital limb reduction.

Assistive technology has revolutionized the lives of individuals with disabilities, offering newfound independence and capability. From simple canes and braces to complex prosthetics and exoskeletons, these devices have provided them with the support needed to live normal lives. According to Precedence Research, the global prosthetics and orthotics market was estimated at USD 9.93 billion in 2021 and is projected to reach over USD 15.42 billion by 2030

Among modern innovations in this field, intelligent robotic systems stand out as promising tools with great potential. Robotic manipulators, designed to seamlessly integrate with wheelchairs, present a particularly compelling solution for individuals that suffer from upper limb disabilities. Products such as the Kinova Jaco are multipurpose devices that aim to help perform simple tasks that the patient's limbs are not able to do such as manipulating small objects and pressing buttons. While they are promising and increase the quality of life of the patient greatly, such products pose challenges as their extremely high prices are unaffordable to most people in the third world. Another challenge is the control device for these manipulators are joysticks which have numerous buttons and are very difficult to control. We aim to tackle both these challenges in our project.

Figure 1 Kinova Jaco, the inspiration behind our project

ROBOTIC MANIPULATORS

In this thesis, our focus lies in the design and fabrication of an intuitive robotic manipulator tailored for assistive use by individuals with upper limb disabilities. The manipulator, equipped with an EMG and IMU based control system, aims to enable them to accomplish tasks that might otherwise be challenging or impossible. From grasping objects to performing movements, the manipulator's versatility is intended to enhance users' quality of life by promoting autonomy and accessibility.

This project encompasses a multi-step process, including mechanical design, electronic integration, and programming tailored to the unique needs of the target user group. Emphasis is placed on safety, reliability, and user-friendliness. By bridging the gap between technology and accessibility, this endeavor seeks to redefine possibilities for individuals with upper limb disabilities, fostering greater inclusion and empowerment in their daily experiences.

A key motivation behind this project is to reduce the costs associated with assistive technology. Currently, the rehabilitative products available in the global market are prohibitively expensive due to the associated product research lifecycle as well as the use of state-of-the-art composite materials and electronics. As such, widespread adoption of such devices in the Global South is hampered due to the high barrier of entry. By employing off-the-shelf electronics and additive manufacturing for fabrication of the device, we aim to keep the cost as low as possible, keeping in mind the target market.

Relying on 3D printed parts and low-cost commercially available Chinese electronics would be the key to reducing costs, making assistive robots viable for the Global South.

TELEOPERATION POSSIBILITIES

Apart from this particular use case, robotic manipulators are being employed in various industries, such as manufacturing, packaging, assembly, and welding. The manipulator fabricated from this project can be used for various other applications and the novel control system will help pave the way to the future of robot teleoperation.

CHAPTER 2: LITERATURE REVIEW

Based on our study of the existing work on rehabilitative models, we developed a framework of the desired control strategies. The control of the manipulator itself can be achieved via PID control for a 4 DoF robotic manipulator using D-H parameters/ The actuation systems being used in commercial applications heavily favour DC motors (Desplenter et al., 2020) there are novel actuation models being introduced—especially in novel soft robotics applications. *(See figure 2)*

Figure 2 Classification of commercially available assistive robotic actuation strategies..
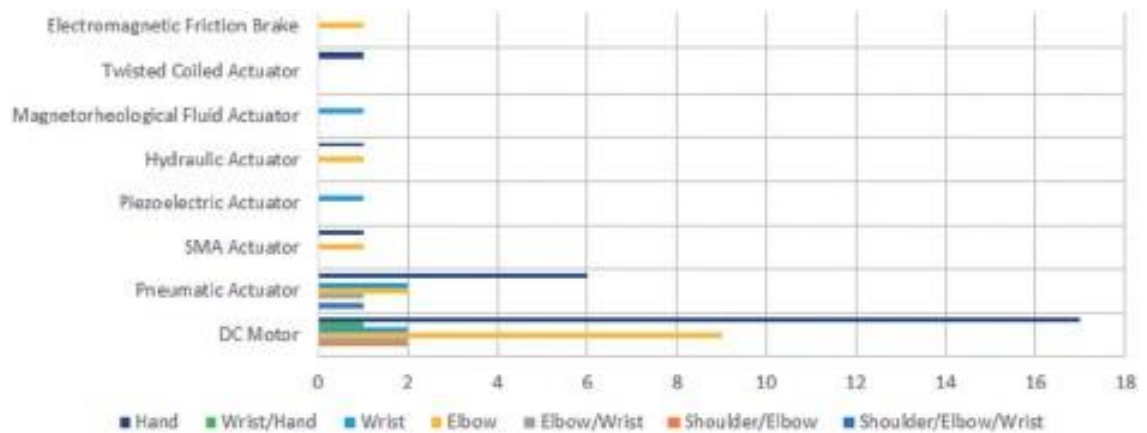
Pneumatic actuators offered a promising alternative to traditional DC/Electromagnetic actuators and were considered for our robot due to their low weight and conformability. However, the lack of available Proportional Control Valves and economic infeasibility of importing the aforementioned control valves restricted the implementation.

Table 1: The decision matrix for the selection of the actuators

Actuators	Manufacturability	Cost	Speed	Mobility	Accuracy	Weight	Total
PNEUMATIC	7	2	7	9	7	10	42
ELECTROMECHANICAL	5	7	7	7	9	6	41
HYDRAULIC	4	5	8	3	8	4	32

:

The scores were assigned to each actuator via a thorough analysis of papers using such models (Design and Analysis of six DOF Robotic Manipulator 2021) (Simple and Scalable Soft Actuation Through Coupled Inflatable Tubes 2022) (Design and Analysis of six DOF Robotic Manipulator 2021) (A Hollow Polyethylene Fiber-Based Artificial Muscle 2019) (Sareh & Rossiter, 2013). The consensus was that while pneumatic actuators tend to perform better across all performance parameters, the prohibitive cost is a significant hindrance in justifying its implementation for our particular use-case. Hydraulically actuated robots perform the worst for small scale robots owing to the manufacturing complexities and increased wight penalties making them uniquely suited to industrial applications. (Pajak & Pajak, 2021)

Pneumatic actuators are being widely incorporated in modern assistive rehabilitative robotics due to their conformability and lightweight construction making them ideal for wearable applications. (Lee & Rodrigue, 2019). The benefits are not suitably offset by the high cost of proportional valves to justify the investment. In either case, the electromagnetic actuators allow for closed loop control at a significantly reduced costs with minimal drawbacks in manufacturability.(Lee & Rodrigue, 2019)

Liu and Wei used a simple servo-actuated robot capable of lifting limited loads. The discussions of Wei and Liu mentioned the possibility of incorporating belt and pulley

mechanisms and harmonic reducers in conjunction with larger stepper motors to further improve the load capacity for industrial/teleoperation applications.(Qiuyue Wei et al., 2019) Our goal was then to analyze the feasibility of multiple actuation strategies to ensure a compact yet robust manipulator capable of meeting the following criteria:

Table 2: Selection matrix for Drive Mechanism

Types of Gear	Manufacturability	Cost	Space Constraint	Slippage	Accuracy	Weight	Total
CYCLOIDAL	3	2	7	9	10	4	35
PLANETARY	8	7	7	9	9	6	46
BELT DRIVEN	10	9	3	3	2	10	37

A comparison of the gearboxes was made according to publicly available data from robotics and mechanical engineering textbooks (Shigley's Mechanical Engineering), Belt driven mechanisms tended to be complicated and open, leading to possible issues with jams. Cycloidal gears are the best possible in terms of performance but the complex assemblies and added weight make it unfeasible to perform at scale. The planetary gearbox performs the best across all considered matrices, providing a good reduction ratio with minimal issues with printing. (*See Table 2*)

The data will be collected from the user via Thalmic Labs' Myoband. The 8 channels of EMG signals detected by the Myo armband are passed via Bluetooth to the Raspberry Pi where all channels of signals are classified to detect the hand gestures. (Biomedical

applications of soft robotics 2018) The Myo armband consists of 8 EMG sensors with high

sensitive nine-axis IMU containing a three-axis gyroscope, three-axis accelerometer, and

a three-axis magnetometer(Bisi et al., 2018). (see fig)

Figure 3 Thalmic Labs MyoBand

The positional data is collected from the integrated IMU and processed to provide real time

updates on limb movement.(da Silva et al., 2020) (*See Figure 4*)

Figure 4 MatLab Visualiser for EMG Data and IMU limb Movement
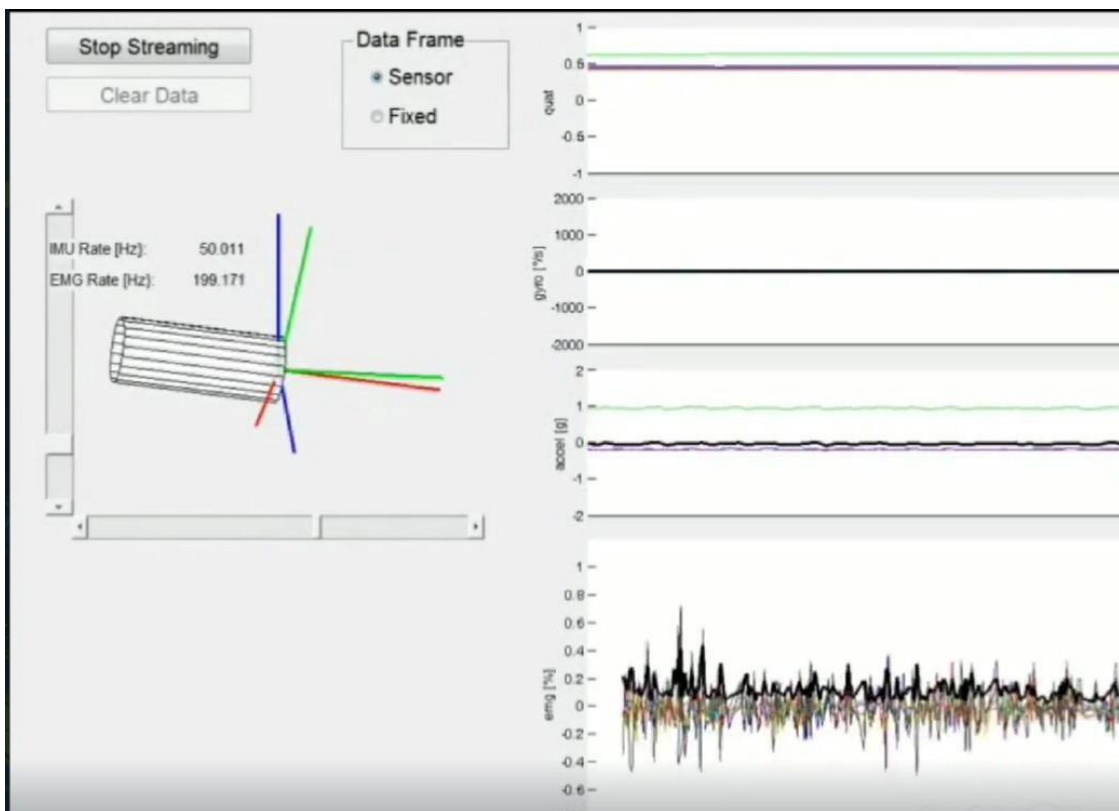
CHAPTER 3: METHODOLOGY

MATERIAL SELECTION:

We considered several 3D printing materials commonly used in robotics and narrowed it down to three main choices: Polylactic Acid (PLA), Acrylonitrile Butadiene Styrene (ABS), and Polyethylene Terephthalate Glycol (PETG). Amongst these, PLA distinguished itself through its widespread availability, user-friendly printing characteristics, and cost-effectiveness. After a comprehensive evaluation of all candidate materials detailed in subsequent sections (*See Table 2b*), PLA emerged as the optimal choice for constructing the robotic manipulator.

PLA:

PLA's prevalence in 3D printing stems from its favorable physical and environmental properties. Its low toxicity and minimal odor emission during printing render it a non-hazardous choice for robots interacting with humans or operating in enclosed spaces. Additionally, PLA exhibits commendable mechanical strength and stiffness, making it suitable for fabricating functional robot components subject to moderate mechanical loads. Furthermore, its inherent biodegradability aligns with increasing environmental concerns, offering a sustainable alternative to non-degradable materials.

However, limitations exist regarding PLA's thermal and impact resistance. Elevated temperatures exceeding its glass transition temperature (Tg) can induce undesirable deformation and potential loss of structural integrity. While suitable for typical indoor operating environments, PLA is not be well-suited for applications involving high heat exposure. (Handling hot beverages etc)

ABS:

ABS is a robust thermoplastic that boasts superior strength, durability, and heat resistance. Ideal for robots facing high temperatures or impacts, its dimensional stability ensures precise part assembly. However, warping and cracking during printing necessitate meticulous control, exceeding the scope of our readily available resources. It also emits harmful fumes during printing which necessitates an enclosed ventilation system, adding

complexity and potential environmental concerns. Despite these challenges, ABS remains a top choice for demanding robotic components.

PETG:

PETG offers a unique combination of strength and flexibility, making it well-suited for parts requiring controlled bending or dynamic loading. This characteristic can be advantageous in applications involving specific environmental demands due to its inherent chemical and moisture resistance. Additionally, superior layer adhesion compared to ABS enhances the overall integrity of fabricated parts.

However, it's crucial to note that meticulous calibration and attention to printing parameters are vital for achieving optimal results with PETG. While exhibiting less warping than ABS, it still demands precision to ensure pristine finishes. Furthermore, its slightly lower overall strength compared to PLA poses a limitation depending on specific load requirements within the project.

Table 2b: Filament Material Comparison

	PLA	ABS	PETG
Density	1.25 g/cm^3	1.04 g/cm^3	1.27 g/cm^3
Yield Strength	28.08 MPa	24 MPa	47.9 MPa
Ultimate Tensile Strength	32.9 MPa	29 MPa	60 MPa
Young's Modulus	3.5 GPa	2.4 GPa	1.3 GPa
Poisson's Ratio	0.332	0.37	0.38

3D PRINTING CONSIDERATIONS:

During 3D printing there are certain parameters that can affect the quality of the product. The STL files of the CAD models of the individual parts need to be sliced to generate G-Codes which are read by the printer. Slicing software used by us is 'Ultimaker Cura'. Following parameters are kept in check to ensure our desired quality:

- Infill density
- Support density
- Horizontal expansion
- Wall thickness
- Print speed
- Bed adhesion
- Layer height

The versatility of 3D printing allows us to create complex and intricate designs with the use of support structures. These temporary structures are essential for printing overhanging features, intricate geometries, and bridges that would otherwise collapse during the printing process.

A critical aspect of this strategy involves understanding the inherent characteristics of the filament being used. While filament layers generally demonstrate remarkable strength in the radial direction, the bond between layers in the axial direction can be significantly weaker, making the printed part more susceptible to splitting along these lines. This characteristic necessitates careful part orientation during the design phase. By strategically positioning the part, we can ensure that forces and stresses primarily act in the strong radial direction, minimizing the need for extensive support structures and optimizing the part's overall strength.

In short, achieving successful and efficient 3D printing requires considering numerous factors beyond simply the design itself. Understanding the implications of supports, the importance of part orientation, and the inherent properties of the filament are all crucial aspects of the process. By carefully considering these elements during the design phase, we can ensure that our printed parts exhibit the desired strength and functionality while optimizing production time and minimizing material waste.

For printing, we'll be using a custom made printer with a build volume of 210x210x210 mm.

MECHANICAL COMPONENTS:

The assembly of our robotic manipulator consists of the following members:

- Base
- Arm Assembly
- End effector (gripper)

Figure 5 Assembled and disassembled planetary gearboxes

`

DESIGN ITERATIONS:

The assembly has been altered many times with modifications according to our needs each time. Simulation based testing has been done on our designs and we adapted the design accordingly. Starting from preliminary hand-drawn designs and after numerous modifications, we have finalized a design which exceeds our expectations during simulation results and only then we started on its manufacturing.

Figure 6-8: (*clockwise, from top left)* preliminary design of manipulator with Sg 90 Servos, intermediate design for Simulink Simulations (Simscape), Finalised design render after revisions
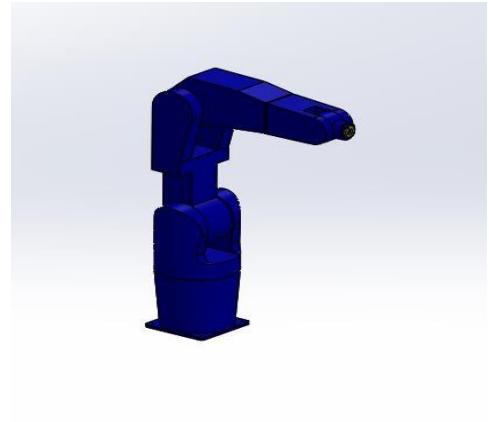
The short comings in the preliminary design included less-space housing space for electronics and wirings, low payload delivery, less torque and limited range due to servos.

These were refined in intermediate design by employed stepper motors instead of servos coupled with cycloidal gearing. However, this assembly was increased or weight significantly (by 350 grams per gear—nearly a kilogram of extra weight), and 3D printed parts showed great deflections due to links being made of compliant material.

The issues were further sorted out in final design where we incorporated planetary gear system instead of cycloidal which reduces the complexity of the assembly, reduces the weight, and is cheaper to manufacture. To counter the deflection problem, we plan to use carbon fiber rods which are light and have higher load bearing capacity.

Furthermore, high torque NEMA 17 stepper motors were used for base and the shoulder joint while a medium torque NEMA 17 was utilized for the elbow joint.

The data sheets for the stepper motors being used are as follows (*See table 3 and 4*):

Table 3 NEMA 17 Datasheet

Description	Length	Mounted Rated Current	Mounted Holding Torque		Winding		Detent Torque		Rotor Inertia		Motor Weight	
					Ohms	mH						
(Stack)	"L" Max	Amps	Nm Typ.	oz-in Typ.	±10% @ 20°C Typ.		mNm	oz-in	g cm2	oz-in2	kg	lbs
Single	39.8 mm (1.57 in)	2	0.48	68	1.04	2.2	15	2.1	57	0.31	0.28	0.62
Double	48.3 mm (1.90 in)	2	0.63	89	1.3	2.9	25	3.5	82	0.45	0.36	0.79
Triple	62.8 mm (2.47 in)	2	0.83	120	1.49	3.8	30	4.2	123	0.67	0.6	1.3

Table 4 NEMA 23 Datasheet

Step Angle	1.8° (+/-5%@ full step, no load)
Resistance Accuracy	+/-10%
Inductance Accuracy	+/-20%
Temperature Rise	80DegreeC MAX.
Ambient Temperature	-20 ~ +50 DegreeC
Shaft Radial Play	0.02MAX @ 450g-load
Shaft Axial Play	0.08MAX @ 450g-load
MAX Radial Force	75N @ 20mm from the flange
MAX Axial Force	15N
Dielectric Strength	500VAC for one minute
Insulation Resistance	MIN 100Mohms, 500VDC

`

DYNAMICS:

In the realm of robotics, dynamics is the study of how forces govern a robot's motion. Essentially, it delves into understanding how external forces acting on the robot's intricate mechanisms translate into its movements and accelerations.

For analysis, the robot's structure is often simplified by treating it as a rigid body system. This allows us to leverage the established principles of rigid body dynamics. However, the resulting equations of motion, describing the robot's precise movements based on various variables, can become quite complex. The equation of motion of a manipulator can be written as:

$$M(q)q \quad \dot{q}^T C(q)\dot{q} = r + r_g(q)$$

Where M(q) is the nxn inertial matrix, holding the inertia values of each robot link,

C(q) is the nxnxn Coriolis tensor,

τ is the n-dimensional vector of the torsions of the actuated joints,

$\tau_g(q)$ is the n-dimensional vector of the torsion at joints due to gravity

INVERSE DYNAMICS:

Manipulator inverse dynamics, at its core, calculates the joint forces and torques required for a robot to achieve a specific motion path. This path is defined by a series of joint positions, velocities, and accelerations.

Understanding these calculations empowers us in two key areas: robot control and trajectory planning.

- Control: Inverse dynamics becomes an integral part of the feedback or feedforward loop, translating desired positions, velocities, and accelerations (derived from a predetermined trajectory) into the necessary joint forces that drive the robot's movement.

- Trajectory Planning: This technique allows us to verify the feasibility of a proposed trajectory, ensuring it can be executed within the limitations of the robot's actuators.

Two widely used methods for calculating inverse dynamics are the Newton-Euler method and the Lagrange method. In our project, the RNE (Recursive Newton-Euler) method, implemented within MATLAB, proved effective for analyzing the inverse dynamics.

FORWARD DYNAMICS:

A branch of robot dynamics that involves numerically calculating the joint accelerations of a robot as a function of its current joint positions, velocities, and the torques applied by its actuators. This method is widely used in robot control system simulations to predict and verify robot behavior under various control inputs. It is calculated using robotics toolbox in MATLAB.(Murray et al., 1994; Spong et al., n.d.)

KINEMATICS:

A commonly used convention for selecting frames of reference in robotic applications is the Denavit-Hartenberg, or DH convention. In this convention, each homogeneous transformation Ai is represented as a product of four basic transformations.

$$
\begin{aligned}
A_i &= Rot_{z,\theta_i} \, Trans_{z,d_i} \, Trans_{x,a_i} \, Rot_{x,\alpha_i} \\
&= \begin{bmatrix} c_{\theta_i} & -s_{\theta_i} & 0 & 0 \\ s_{\theta_i} & c_{\theta_i} & 0 & 0 \\ 0 & 0 & 1 & 0 \\ 0 & 0 & 0 & 1 \end{bmatrix} \begin{bmatrix} 1 & 0 & 0 & 0 \\ 0 & 1 & 0 & 0 \\ 0 & 0 & 1 & d_i \\ 0 & 0 & 0 & 1 \end{bmatrix} \\
&\quad \times \begin{bmatrix} 1 & 0 & 0 & a_i \\ 0 & 1 & 0 & 0 \\ 0 & 0 & 1 & 0 \\ 0 & 0 & 0 & 1 \end{bmatrix} \begin{bmatrix} 1 & 0 & 0 & 0 \\ 0 & c_{\alpha_i} & -s_{\alpha_i} & 0 \\ 0 & s_{\alpha_i} & c_{\alpha_i} & 0 \\ 0 & 0 & 0 & 1 \end{bmatrix} \\
&= \begin{bmatrix} c_{\theta_i} & -s_{\theta_i} c_{\alpha_i} & s_{\theta_i} s_{\alpha_i} & a_i c_{\theta_i} \\ s_{\theta_i} & c_{\theta_i} c_{\alpha_i} & -c_{\theta_i} s_{\alpha_i} & a_i s_{\theta_i} \\ 0 & s_{\alpha_i} & c_{\alpha_i} & d_i \\ 0 & 0 & 0 & 1 \end{bmatrix}
\end{aligned}
$$

To encapsulate the geometric approach for solving the inverse kinematics equations, a solution to the inverse kinematics of 6 DoF elbow manipulator can be approached as:

Given

$$O = \begin{bmatrix} o_x \\ o_y \\ o_z \end{bmatrix}; \quad R = \begin{bmatrix} r_{11} & r_{12} & r_{13} \\ r_{21} & r_{22} & r_{23} \\ r_{31} & r_{32} & r_{33} \end{bmatrix}$$

then with

$$
\begin{aligned}
x_c &= o_x - d_6 r_{13} \\
y_c &= o_y - d_6 r_{23} \\
z_c &= o_z - d_6 r_{33}
\end{aligned}
$$

a set of DH joint variables is given by

$$\theta_1 = \operatorname{atan2}(x_c, y_c)$$

$$\theta_2 = \operatorname{atan2}\left(\sqrt{x_c^2 + y_c^2 - d^2}, z_c - d_1\right) - \operatorname{atan2}(a_2 + a_3 c_3, a_3 s_3)$$

$$\theta_3 = \operatorname{atan2}\left(D, \pm\sqrt{1 - D^2}\right),$$

$$\text{where } D = \frac{x_c^2 + y_c^2 - d^2 + (z_c - d_1)^2 - a_2^2 - a_3^2}{2 a_2 a_3}$$

$$\theta_4 = \operatorname{atan2}(c_1 c_{23} r_{13} + s_1 c_{23} r_{23} + s_{23} r_{33},$$
$$-c_1 s_{23} r_{13} - s_1 s_{23} r_{23} + c_{23} r_{33})$$

$$\theta_5 = \operatorname{atan2}\left(s_1 r_{13} - c_1 r_{23}, \pm\sqrt{1 - (s_1 r_{13} - c_1 r_{23})^2}\right)$$

$$\theta_6 = \operatorname{atan2}(-s_1 r_{11} + c_1 r_{21}, s_1 r_{12} - c_1 r_{22})$$

FORWARD KINEMATICS:

The forward kinematics are enumerated by calculating the twist motions at each joint. These are given by:

$$\xi_1 = \begin{bmatrix} -\begin{pmatrix} 0 \\ 0 \\ 1 \end{pmatrix} \times \begin{pmatrix} 0 \\ 0 \\ l_0 \end{pmatrix} \\ \begin{pmatrix} 0 \\ 0 \\ 1 \end{pmatrix} \end{bmatrix} = \begin{bmatrix} 0 \\ 0 \\ 0 \\ 0 \\ 0 \\ 1 \end{bmatrix} \qquad \xi_2 = \begin{bmatrix} -\begin{pmatrix} -1 \\ 0 \\ 0 \end{pmatrix} \times \begin{pmatrix} 0 \\ 0 \\ l_0 \end{pmatrix} \\ \begin{pmatrix} -1 \\ 0 \\ 0 \end{pmatrix} \end{bmatrix} = \begin{bmatrix} 0 \\ -l_0 \\ 0 \\ -1 \\ 0 \\ 0 \end{bmatrix}$$

$$\xi_3 = \begin{bmatrix} 0 \\ -l_0 \\ l_1 \\ -1 \\ 0 \\ 0 \end{bmatrix} \qquad \xi_4 = \begin{bmatrix} l_1+l_2 \\ 0 \\ 0 \\ 0 \\ 0 \\ 1 \end{bmatrix} \qquad \xi_5 = \begin{bmatrix} 0 \\ -l_0 \\ l_1+l_2 \\ -1 \\ 0 \\ 0 \end{bmatrix} \qquad \xi_6 = \begin{bmatrix} -l_0 \\ 0 \\ 0 \\ 0 \\ 1 \\ 0 \end{bmatrix}$$

Figure 9 Schematic diagram of manipulator
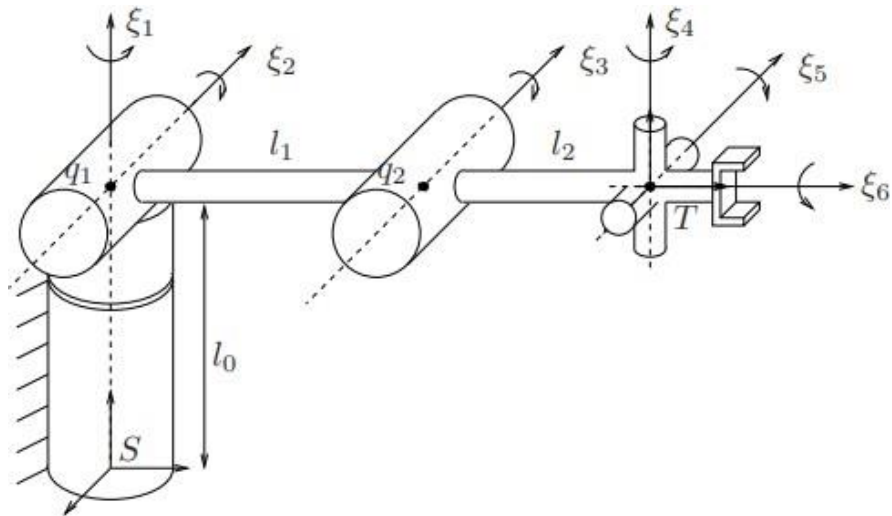
The full forward kinematics are:

$$g_{st}(\theta) = e^{\widehat{\xi}_1 \theta_1} \cdots e^{\widehat{\xi}_6 \theta_6} g_{st}(0) = \begin{bmatrix} R(\theta) & p(\theta) \\ 0 & 1 \end{bmatrix}$$

where

$$R(\theta) = \begin{bmatrix} r_{11} & r_{12} & r_{13} \\ r_{21} & r_{22} & r_{23} \\ r_{31} & r_{32} & r_{33} \end{bmatrix}$$

$$p(\theta) = \begin{bmatrix} -\sin\theta_1 (l_1 \cos\theta_2 + l_2 \cos(\theta_2 + \theta_3)) \\ \cos\theta_1 (l_1 \cos\theta_2 + l_2 \cos(\theta_2 + \theta_3)) \\ l_0 - l_1 \sin\theta_2 - l_2 \sin(\theta_2 + \theta_3) \end{bmatrix}$$

SIMULATION:

To streamline both the control and simulation processes, we leveraged the capabilities of Simulink. This software allowed us to seamlessly import our CAD model, creating a virtual representation of the robot within the simulation environment. Furthermore, for precise control, we implemented inverse kinematics.

SIMULINK:

For seamless development and testing, we opted for Simulink, a MATLAB-based environment ideal for multi-domain simulations. This powerful tool allowed us to import our robot's CAD model and define its kinematics using a combination of specialized robotics toolbox blocks and general utility blocks.

Leveraging these blocks, we then built a virtual representation of the robot, enabling us to simulate its movements by feeding it desired trajectories through readily available trajectory blocks. Simulink essentially served as a virtual testing ground, allowing us to refine our design and control strategies before transitioning to physical hardware.

TRAJECTORY:

Trajectory planning plays a crucial role in robotics, dictating the path a robot's limbs (manipulators) take to reach desired points. It involves calculating the precise joint angles at each point in time, allowing the manipulator to smoothly transition from its starting position to one or multiple target configurations.

Several factors demand careful consideration during this planning process, but none more critical than avoiding singularities. These "blind spots" in a robot's joint space, when encountered, can cause unpredictable and potentially dangerous behavior due to the loss of control over the manipulator. The several trajectories that can be carried out through Simulink include:

- B-spline trajectory
- Polynomial trajectory
- Trapezoidal trajectory

SIMULINK MODEL

Figure 10 Simulink Model of Robot using Simscape and MATLAB Robotics
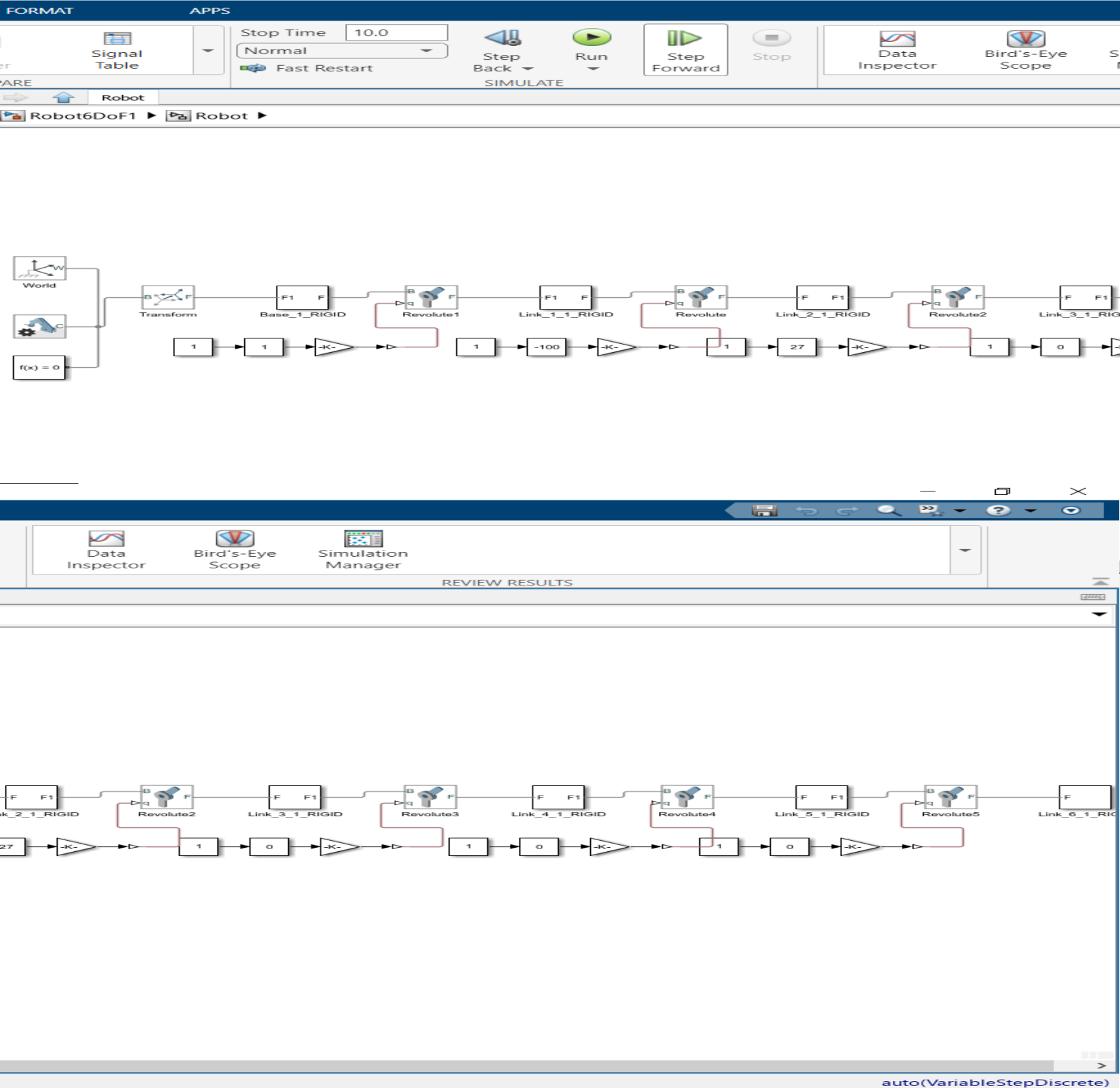
GRIPPER MECHANISM:

The gripper for our model was designed to ensure that it can pick up objects with complex geometries and intricate design and also handle fragile objects without breaking them but also be strong and rigid enough to lift a considerable amount of weight that would be required in everyday usage of a disabled person that the arm is designed for.

The conventional design of most robots often lacks scalability, versatility in control methods and actuation, and flexibility in materials. Additionally, the fabrication and assembly processes for many robots, particularly soft robots, are complex and time-consuming, involving multiple molds and steps that can take a day or more to complete.

To address these challenges, we sought a soft robotic solution that would be straightforward to fabricate and assemble, incorporate a minimal number of actuators, allow scalability in size, and enable easy modification for different materials, control schemes, and actuation methods. The Fin Ray® Effect emerged as the ideal solution meeting all these criteria.

The Fin Ray Effect was originally observed by biologist Leif Kniese of Evologics while fishing, inspired by the deformation of fish fins. In fish fins, the structure consists of two bones arranged in a V shape with connective tissue in between. When one side of the V is pulled, the fin deforms. Kniese adapted this concept into an A-frame structure with crossbeams spaced between the tip and base. Applying a force to this structure causes it to bend. The symmetric design of this structure allows it to bend equally in either direction.

Figure 11 Loaded and Unloaded Fin Ray Gripper
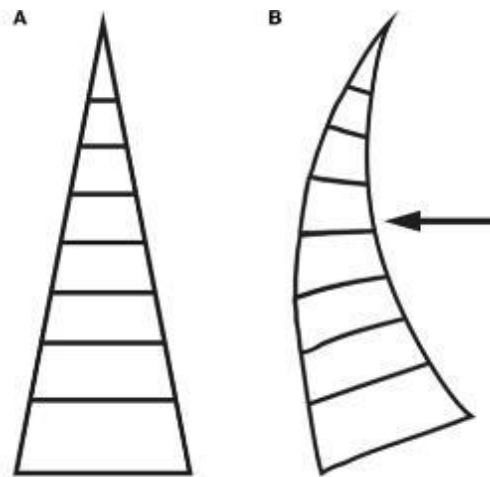
ELECTRONICS:

The design incorporates the use of a limit switch that is used to send signals by completing the circuit at each extreme of the gripper motion which sends a HIGH value to the Arduino Uno board used for gripper control. The code written is fairly straightforward in logic as is the function of the gripper. It senses the HIGH and LOW values from the gripper's limit switch which allows it to confirm if the gripper is open or closed. A L298N motor driver is also used for running the gripper which allows for controlling the speed of the gripper and changing the polarity of the voltage signal.

The L298N is an integrated circuit used for driving DC motors and stepper motors. It features dual H-bridge circuits, allowing control over motor direction and speed. The IC is controlled via logic-level inputs to set motor direction and enable/disable motor outputs. A power supply is used to provide a supply of about 9 – 12 volts to the motor driver.

DESIGN AND MANUFACTURING:

For the actuation of the gripper, an N20 geared DC motor is used which is compact but also powerful enough for this use case. The motor driver provides a DC supply of 5 volts required for the motor.

GRIPPER DESIGN

For the design and manufacturing of the gripper a 3 finned gripping design was used with tests performed to create the best fins that offer high strength while deformed and that wraps around intricate objects without breaking them. The gripper was made through additive manufacturing like the rest of the gripper parts. The material for this gripper was Thermoplastic Polyurethane (TPU) that helps with the deformability of the fins. The fins are also coated with a layer of silicone rubber that is cured on to them and helps increase the friction force that enables the gripper to lift heavier objects.

FILAMENT SELECTION

TPU (Thermoplastic Polyurethane) is a flexible and elastic material used in 3D printing. It offers excellent resilience, impact resistance, and abrasion resistance. TPU is relatively easy to print compared to other flexible materials and adheres well to print beds. It comes in various hardness levels, making it suitable for prototyping and producing functional parts like gaskets, phone cases, and wearable items such as wristbands and sportswear components. When printing with TPU, it's important to use appropriate print settings, including slower speeds and lower layer heights, to achieve good print quality. Overall, TPU is valued for its flexibility and versatility in creating durable, flexible 3D printed objects.

The rest of the parts of the gripper were 3D printed using Polylactic Acid (PLA) with infill set to around 30%. This includes a lead screw that is fastened to the motor shaft using a screw. This lead screw turns with the motor and moves the 3 clamps that hold the fins that

also have teeth on the inside. The mechanism is very similar to a worm gear. The clamps are attached to a base which is then in turn attached to the rest of the robotic manipulator using a mount specifically made for the gripper.

PLA (Polylactic Acid) is a popular 3D printing filament known for its biodegradability and ease of use. Derived from renewable resources, PLA is environmentally friendly and emits a pleasant, sweet smell when printed. It adheres well to print beds and has minimal warping, making it ideal for beginners. PLA offers good detail resolution and comes in various colors and finishes, suitable for prototyping, educational use, art, and household objects. While PLA prints are not heat-resistant, they are safe for indoor use due to low toxicity. Overall, PLA is widely appreciated for its versatility, safety, and suitability across a broad range of 3D printing applications.

CONTROL STRATEGY:

EMG and IMU signals were collected using the Thalmic Labs Myo armband. The device is mounted on the user's forearm and consists of eight surface electrodes with a sampling rate of 200hz and an IMU with a 50hz sampling rate. The data is transferred over Bluetooth to an external computer for processing.

FEATURE RECOGNITION:

The device uses feature extraction to detect particular gestures. The signal is preprocessed by applying filters. Afterwards, consistent patterns that correspond to each gesture are highlighted and used to train the armband's model.
Using this technique, multiple gestures can be detected using the Myo armband and used for actuation purposes.

IMU DATA PROCESSING:

An Inertial Measurement Unit is a device consisting of a set of sensors. They record the linear acceleration, angular acceleration, and orientation of the device at any given moment by employing a gyroscope, accelerometer, and magnetometer.

The IMU allows us to track the movement of the user's arm in Cartesian space and use it to actuate our manipulator accordingly by varying joint angles with the gear ratios and limits incorporated..

PROCESSING AND ACTUATION:

The IMU data received from the Myo armband, is mapped to coordinates using a python script and windows API and these coordinates are sent to the microcontroller using its serial port. The microcontroller then moves the stepper motors to the required coordinates every time a movement is detected by the armband.

The EMG data is read by the proprietary device software to look for gestures. Four different gestures are used for actuation. Two are employed to move the shoulder joint while the other two are used to actuate the end effector. These gestures are then read as ASCII codes by the serial port of the microcontroller and motors are actuated accordingly.

The Appendix contains full excerpts of both the python and the microcontroller code.

CHAPTER 4: RESULTS AND DISCUSSIONS

In order to check whether our gearbox can bear all the stresses during operation, we perform mechanical analysis on our design to see its performance under use. First, we will check the load on our gearing.
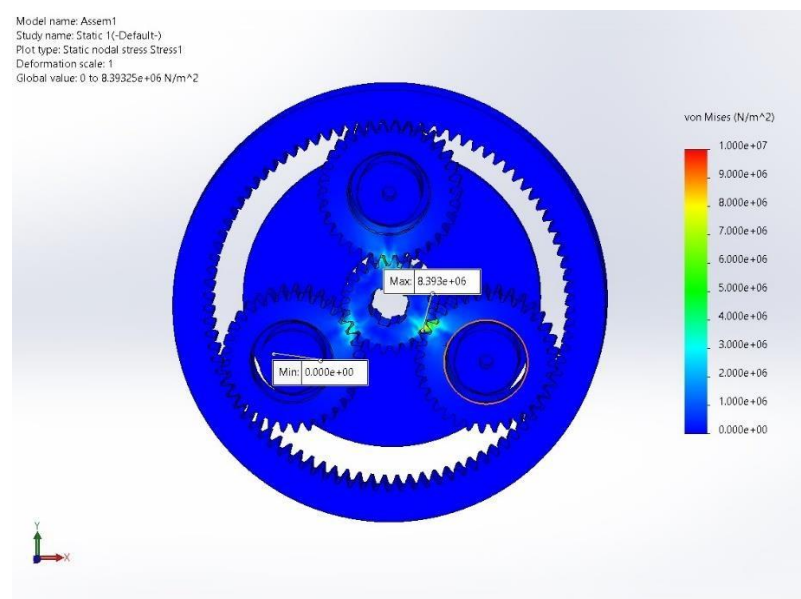
GEARBOXES:

Our gearboxes are additively manufactured to decrease weight and save costs. So it is necessary to check whether they can bear the loads during operation. We imported our models into SolidWorks Simulation and applied the expected loads and constraints.

To obtain a conservative estimate of our gearing strength, we assume that the entire system is stalled and 5Nm of torque (5x the operating torque) is applied to the sun gear. The maximum Von Mises Stress calculated by the system was 8 MPa *(See figure 12)*. This is well within the strength of PLA which is 30MPa at 30% infill.
The maximum strain obtained even in such an extreme case is only 2.9×10^{-3}

Figure 5 Stress analysis of Gearbox using SolidWorks Simulation

Figure 6 Strain analysis of Gearbox using SolidWorks Simulation
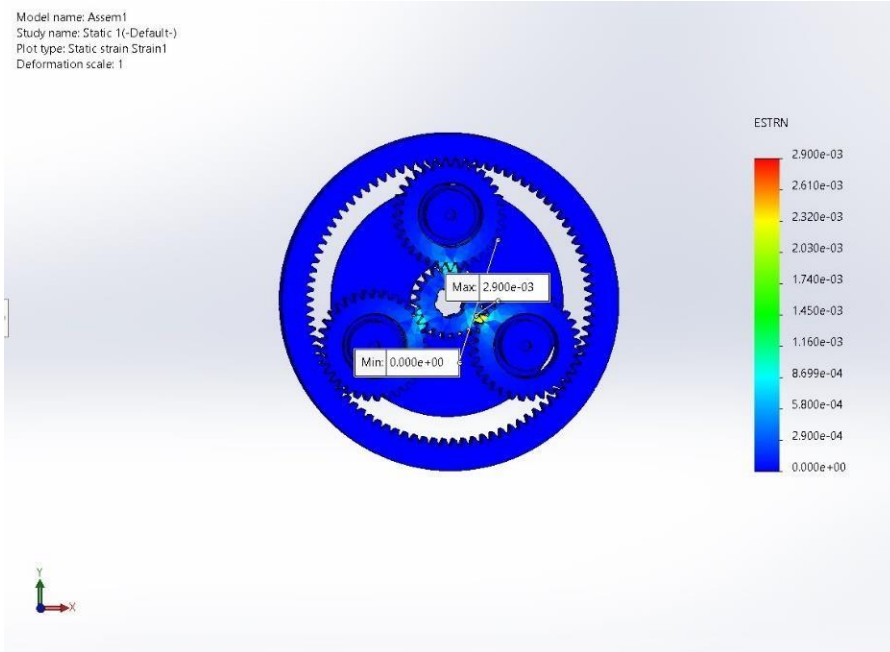
TORQUE CALCULATIONS:

Simple systems can be modeled analytically and do not require FEA software.

We used MathCAD in order to be able to change parameters as the design evolves.

Torque Calculations

Maximum Torque has to be supplied by J1 when all joints are straight and horizontal. The resulting moments can be plotted as

$$a := 250 \; mm$$
$$b := 200 \; mm$$

$$W1 := 0.8 \; kg \cdot g = 7.845 \; N$$
$$W2 := 1.2 \; kg \cdot g$$

$$\theta := 20 \; deg$$
$$\phi := 0 \; deg$$

$$Torque := W1 \cdot a \cdot \cos(\theta) + W2 \cdot (a \cdot \cos(\theta) + b \cdot \cos(\phi)) = 6.961 \; N \cdot m$$

The required torque at j1 is ~7N.m

The available Nema-23 (M1233031) with us has a torque of 1 N.m. Which gives us an approximate gear reduction of 7:1. However, planetary gearboxes have efficiency losses so we should divide the required torque by the efficiency factor to find out the supply torque

$$\eta := 0.7$$

$$T_{supply} := \frac{Torque}{\eta} = 9.945 \; J$$

$$T_{motor} := 1 \; N \cdot m$$

$$i := \frac{T_{supply}}{T_{motor}} = 9.945 \quad \text{~approximately 10:1 gear reduction}$$

DEFLECTION CALCULATIONS:

Length of link: 200mm

Outer Diameter: 25mm

Inner Diameter: 22mm

Bending Load: 10 kg

Deflection: 1.7mm

CHAPTER 5: CONCLUSION AND RECOMMENDATION

The designing and manufacturing of an assistive robotic manipulator that focuses on rehabilitative and mobility technology to provide an intuitive solution to real-world problems faced by people that suffer from upper limb deformities including amyotrophic lateral sclerosis (ALS) and congenital limb deformities was the focus of our project.

ACTUATION MECHANISMS

From conducting our literature review, it was found that for our product's dimensions and purpose the most suitable type of actuator that we can use is an electromechanical actuator rather than pneumatic or hydraulic. The main reasons for this decision are the relatively lower cost and weight, higher speed and accuracy and the fact that it is readily available and easier to assemble due to the compact form factor.

Currently, most rehabilitative medical devices employ brushless DC motors for actuation owing to their high power-to-weight ratio and noiseless operation. While there is growing use of pneumatic actuation due to recent advancements in this technology, there are significant (proportional control valves). Soft Robots and compliant mechanisms inspired by biological systems (Biomimetic Design) offer significant advantages over traditional rigid linkages, however due to the associated costs it was decided not to pursue this form of actuation.

CONTROL STRATEGIES

Our model is heavily inspired by the Kinova Jaco with the difference being that it employs an unintuitive joy-stick control which has a steep learning curve.

Most commercially available rehabilitative robots use EMG signals for sensing employed in a bio-kinematic open-loop control strategy. (Rehabilitative and assistive wearable mechatronic upper-limb devices: A review 2020) Other alternatives use EEG signals and or some sort of combination of both but we settled on using EMG only for control of the manipulator because of the availability of a myoband provided by our supervisor.

The myoband is used to read and process the stimulus from the movement provided by the user to provide two sets of data signals, IMU and EMG. Where IMU provides data on the acceleration, orientation and the angular rates and EMG measures muscle activation which are then processed by the system microprocessor which uses the concept of feature extraction and machine learning to classify received signals to motor actuation.

The control strategy employs a MyoBand which has been provided to us by our supervisor to wirelessly control the robotic manipulator. However, it has 8 sEMG (Surface EMG) electrodes, most of which are not required for our purpose. If we have to make our product commercially viable, we need to reduce the cost and for which we have to make our own control device which consists of a Bluetooth module, 3 surface EMG electrodes and an IMU since we are using only these components from the MyoBand.

MANUFACTURING AND ASSEMBLABILITY

The manipulator has four degrees of freedom with each joint being revolute except the last which actuates the compliant gripper. The manipulator was made using a combination of 3D printing utilizing Rapid Prototyping FDM process with the material being used is a high strength thermoplastic (PLA) which offers refined surface finish and has reasonable impact strength for our use case. This 3D printed PLA is used for the gearing and the casing of the gears. The end effector in use is an adaptive fin gripper that is made of a flexible, compliant TPU core with an external, conformable skin made of silicon. From our calculations and practically it is not suitable to use PLA for the initial linkages as the torque experienced is relatively high therefore we opted for using carbon fiber rods that offers strengthening and support.

For the drive system, we are using NEMA 17 Stepper motors which are driven by the stepper motor driver DRV 8825 for high torque for the initial three joints of our manipulator as the torque requirement is higher.

For the drive mechanism, we used a planetary gear reduction for precision, slippage prevention and torque transmission. We considered three viable options for the mechanism which included planetary, cycloidal and belt driven gearing. The problem with belt driven gearing is that it is not as compact as the other two which is an even bigger problem at higher gear ratios and there is possibility of slippage.

Cycloidal gearing was a viable option and was considered because of its compact nature and we also made a CAD model for additive manufacturing however the degree of precision required for a cycloidal gearing was not feasible due to highly specific geometry and an additional issue of requirement of a multitude of bearings to function which increases the weight of the gearing mechanism considerably. (Design and Analysis of six DOF Robotic Manipulator 2021)

We opted for planetary gearing which offers high torque in a compact design without adding considerable weight which was a major problem for joints 1 and 2. The only drawback with the planetary gearing is that it is not back drivable which can lead to more stress on the gears when an accidental load is applied on the manipulator body. This is not a substantial issue for our product, but it can be improved by using a cycloidal or harmonic gear instead, but it will increase the cost and weight significantly.

DESIGN FOR ASSEMBLY (DFA)

The manipulator was designed with DFM principles in consideration. Each gearbox incorporates notches and counterbore/countersink screwswhere required to ensure ease of assembly. In order to reduce part count, a slew bearing was incorporated into the gearbox itself. This reduced our weight and significantly improved DFA as bearings require precise tolerances, usually difficult with the FDM process. The design uses metric screws throughout to ensure uniformity. Bolts employed were M3/M4 in 6 varying lengths. The uniformity allowed for significantly reduced our inventory count and cross functional parts across the assembly.

DESIGN FOR ADDITIVE MANUFACTURING (DFAM)

Various hurdles were encountered in the process of Additively Manufacturing parts. The unforeseen consequences included the loss of part integrity due to axial forces along the print layer. As the assembly was designed to press fit shafts, these parts would fail along the weaker axial direction. Once the weakness was identified, all parts were redesigned and printed to ensure maximum forces would be distributed along the radial direction of printing filament. This led to improved performance and ease of assembly. Another oversight was inability to account for expansion factors post-printing. Despite using normal tolerance ranges of 0.1-0.3 mm, the expansion due to heated printed beds and non-uniform weight distribution necessitated filing for smooth mates. We were unable to find relevant literature on expansion in various printing methods and filaments, so it could be a viable research project for future researchers.

FUTURE POSSIBILITIES:

This is a modest model and has upscaling possibilities. Some of the features which we plan

to implement include:

- Making the gearboxes out of metal, likely aluminum due to its lightweight and non-corrosion potential.
- Providing more power to the motors for smoother and faster functioning and removing any lag.
- Adding an inverse kinematic closed loop model using encoders to move the gripper more accurately and have the joints orient themselves.
- Increasing the DoF from 4 to 6 to provide more flexibility and ease of movement to the user.
- Redesigning the motor casings to allow more airflow for cooling purposes.
- Building an onboard control unit to incorporate a Raspberry Pi 4 within the robot as the main processor instead of relying on external computing resources.

REFERENCES

Ahn, B., Ko, S. Y., & Yang, G. H. (2020). Compliance control of slave manipulator using EMG signal for telemanipulation. Applied Sciences (Switzerland), 10(4). https://doi.org/10.3390/app10041431

Bisi, S., de Luca, L., Shrestha, B., Yang, Z., & Gandhi, V. (2018). Development of an EMG-controlled mobile Robot. Robotics, 7(3). https://doi.org/10.3390/robotics7030036

Cianchetti, M., Laschi, C., Menciassi, A., & Dario, P. (2018). Biomedical applications of soft robotics. In Nature Reviews Materials (Vol. 3, Issue 6, pp. 143–153). Nature Publishing Group. https://doi.org/10.1038/s41578-018-0022-y

da Silva, L. D. L., Pereira, T. F., Leithardt, V. R. Q., Seman, L. O., & Zeferino, C. A. (2020). Hybrid impedance-admittance control for upper limb exoskeleton using electromyography. Applied Sciences (Switzerland), 10(20), 1–19. https://doi.org/10.3390/app10207146

Desplenter, T., Zhou, Y., Edmonds, B. P., Lidka, M., Goldman, A., & Trejos, A. L. (2020). Rehabilitative and assistive wearable mechatronic upper-limb devices: A review. Journal of Rehabilitation and Assistive Technologies Engineering, 7, 205566832091787. https://doi.org/10.1177/2055668320917870

Fleischer, C., Wege, A., Kondak, K., & Hommel, G. (2006). Application of EMG signals for controlling exoskeleton robots. Biomedizinische Technik, 51(5–6), 314–319. https://doi.org/10.1515/BMT.2006.063

Gao, P., Li, J., & Shi, Q. (2019). A Hollow Polyethylene Fiber-Based Artificial Muscle. Advanced Fiber Materials, 1(3–4), 214–221. https://doi.org/10.1007/s42765-019-00019-6

Kanik, M., Orguc, S., Varnavides, G., Kim, J., Benavides, T., Gonzalez, D., Akintilo, T., Cem Tasan, C., Chandrakasan, A. P., Fink, Y., & Anikeeva, P. (n.d.). Strain-programmable fiber-based artificial muscle. http://science.sciencemag.org/

Lee, J. G., & Rodrigue, H. (2019). Origami-Based Vacuum Pneumatic Artificial Muscles with Large Contraction Ratios. Soft Robotics, 6(1), 109–117. https://doi.org/10.1089/soro.2018.0063

Pajak, I., & Pajak, G. (2021). Motion planning for a mobile humanoid manipulator working in an industrial environment. Applied Sciences (Switzerland), 11(13). https://doi.org/10.3390/app11136209

Park, Y. J., Ko, M. G., Jamil, B., Shin, J., & Rodrigue, H. (2022). Simple and Scalable Soft Actuation Through Coupled Inflatable Tubes. IEEE Access, 10, 41979–41989. https://doi.org/10.1109/ACCESS.2022.3167964

Pratheep, V. G., Chinnathambi, M., Priyanka, E. B., Ponmurugan, P., & Thiagarajan, P. (2021). Design and Analysis of six DOF Robotic Manipulator. IOP Conference Series: Materials Science and Engineering, 1055(1), 012005. https://doi.org/10.1088/1757-899x/1055/1/012005

Qiuyue Wei, , , Yufan Liu, Guangyuan Zhao, Bo Shang, Yun Yan, & Yue Hue. (2019). Design of the Controlling System of a Six-DoF Manipulator. IEEE Symposium Series on Computational Intelligence (SSCI), 2874–2878.

Sareh, S., & Rossiter, J. (2013). Kirigami artificial muscles with complex biologically inspired morphologies. Smart Materials and Structures, 22(1). https://doi.org/10.1088/0964-1726/22/1/014004
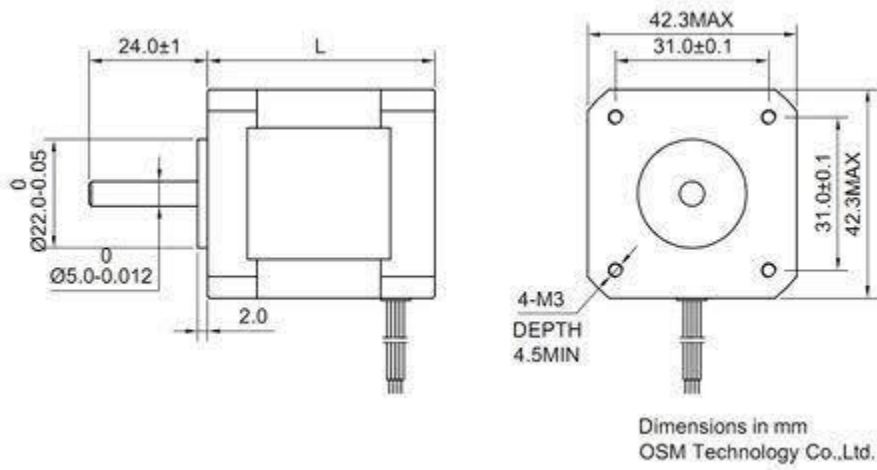
Murray, R. M., Li, Z., & Sastry, Shankar. (1994). A mathematical introduction to robotic manipulation. CRC Press.
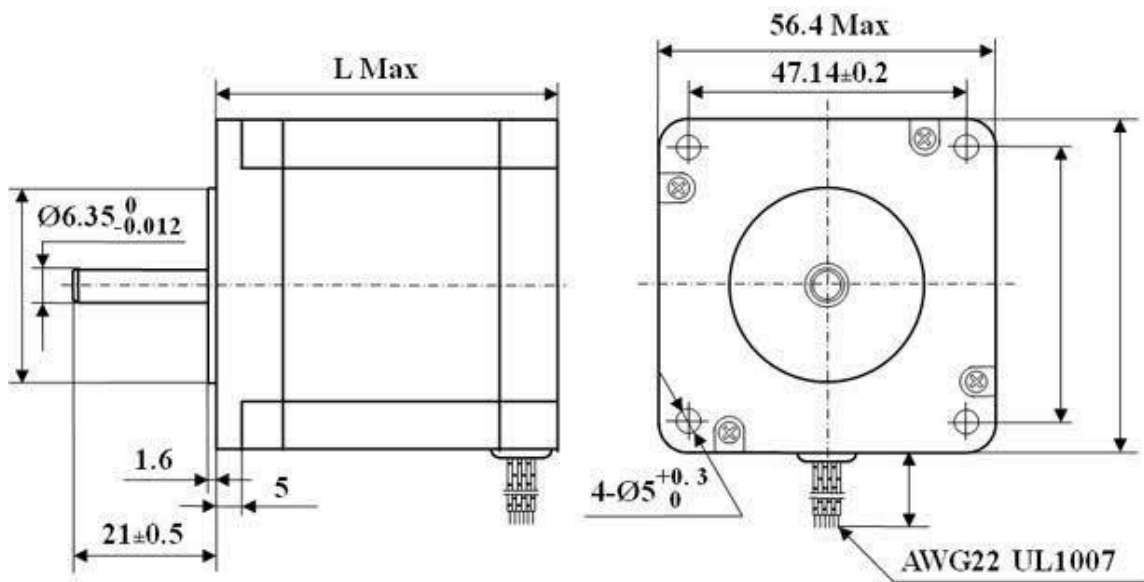
Spong, M. W., Hutchinson, S., & Vidyasagar, M. (n.d.). Robot Modeling and Control First Edition.

APPENDIX I:

Figure A NEMA 17 Dimensions

Figure B NEMA 23 Dimensions

Figure C DRV8825 Stepper Driver Schematic

```python
import pyautogui
import keyboard
import time
import serial

ser=serial.Serial('COM5',9600) #adjust COM port

def send_keys(key_name):
    print(key_name)
    ser.write(f'Key:{key_name}\n'.encode())


def track_cursor():
    while True:
        x, y = pyautogui.position()
        send_coordinates(x, y)
        time.sleep(0.1)

def handle_keyboard():
```

```
    while True:
        key = keyboard.read_event(suppress=True)
        if key:
            send_keys(key.name)

try:
    handle_keyboard()
except KeyboardInterrupt:
    print("Exiting.")
```

Figure D Shoulder Control python code

```
import pyautogui
import serial
import time

#modify the COM number as required
port = serial.Serial('COM4', 9600)

def send_coordinates(x, y):
    port.write(f"{x},{y}\n".encode())  #pass as string
    X=x-960
    Y=-y+540
    print(X,Y)
try:
    while True:
        x, y = pyautogui.position()
        send_coordinates(x, y)
        #delay
        time.sleep(0.1 )

except KeyboardInterrupt:
    print("Exiting.")
    port.close()
```
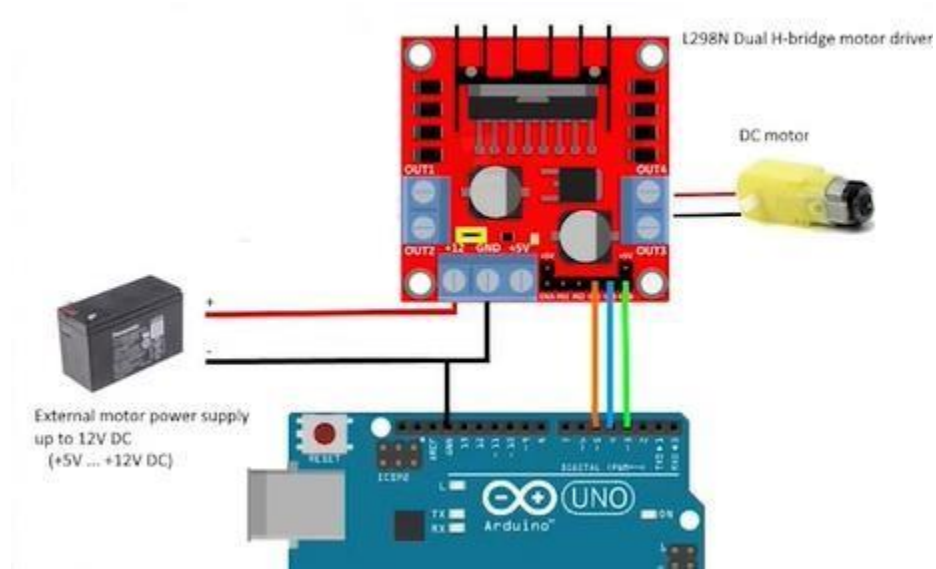
Figure E Base and Elbow Control python codee

```
#include <AccelStepper.h>

// Define the number of steps per revolution for your stepper motor
const int stepsPerRevolution = 200;

// Define the motor pins
const int stepPin1 = 3;
const int dirPin1 = 2;

const int stepPin2 = 5;
const int dirPin2 = 4;

// Initialize the AccelStepper object
AccelStepper stepper1(1, stepPin1, dirPin1);
AccelStepper stepper2(1, stepPin2, dirPin2);

void setup() {
  // Set the speed and acceleration of the stepper motor
  stepper1.setMaxSpeed(500); // Adjust speed as needed
  stepper1.setAcceleration(500); // Adjust acceleration as needed
```

```
    stepper2.setMaxSpeed(500); // Adjust speed as needed
    stepper2.setAcceleration(500);

    // Initialize serial communication
    Serial.begin(9600);
}

void loop() {
    // Check if data is available to read from serial port
    if (Serial.available() > 0) {
        // Read the X and Y positions of the cursor
        String data = Serial.readStringUntil('\n');
        int commaIndex = data.indexOf(',');
        if (commaIndex != -1) {
            int xPos = data.substring(0, commaIndex).toInt();
            int yPos = data.substring(commaIndex + 1).toInt();

            // Map the X and Y positions to the stepper motor rotation
            int xMapped = map(xPos, -960, 959, -4000, 4000); // Adjust 1920
based on your screen resolution
            int yMapped = map(yPos, -540, 540, -4000,4000); // Adjust 1080 based
on your screen resolution

            // Set target position for stepper 1
            stepper2.moveTo(xMapped);

            // Set target position for stepper 2
            stepper1.moveTo(yMapped);
        }
    }

    // Continuously run the stepper motors
    stepper1.run();
    stepper2.run();
}
```

Figure F Base and Elbow Control Arduino code

```
#include <AccelStepper.h>

// Define the number of steps per revolution for your stepper motor
const int stepsPerRevolution = 200;
```

```
// Define the motor pins

const int stepPin3 = 3 ;
const int dirPin3 = 2 ;

// Initialize the AccelStepper object
AccelStepper stepper3(1, stepPin3, dirPin3);

void setup() {
  // Set the speed and acceleration of the stepper motor
  stepper3.setMaxSpeed(500); // Adjust speed as needed
  stepper3.setAcceleration(500);

  // Initialize serial communication
  Serial.begin(9600);
}

void loop() {
  // Check if data is available to read from serial port
  if (Serial.available() > 0) {
    // read incoming command
    String command = Serial.readStringUntil('\n');
    command.trim();
    //to check if the command is keystroke
    if (command.startsWith("Key:"))
    {
      //extract key name
      String keyName = command.substring(4);

      //control movement of motor depending on key value
      if (keyName=="w")
      {
        //move motor forward
        stepper3.move(200);
        stepper3.runToPosition();
      }
      else if(keyName=="s")
      {
        //move motor backward
        stepper3.move(-200);
        stepper3.runToPosition();
      }
```
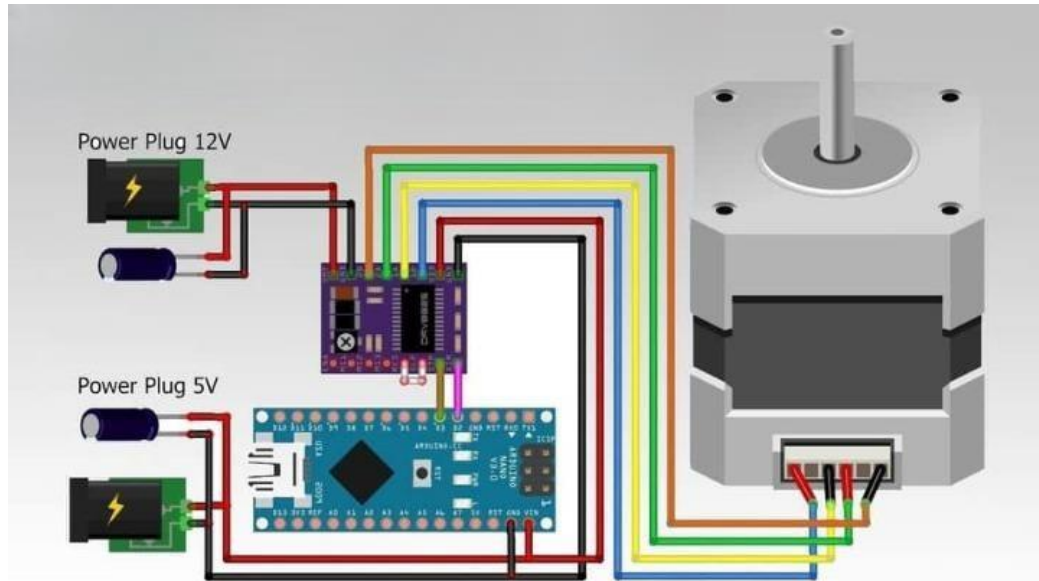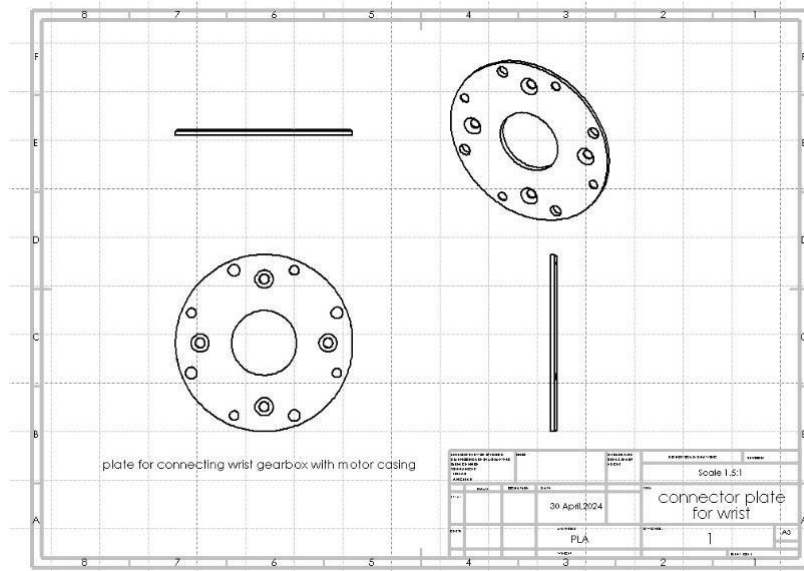
```
    }
    stepper3.run();
    }
}
```

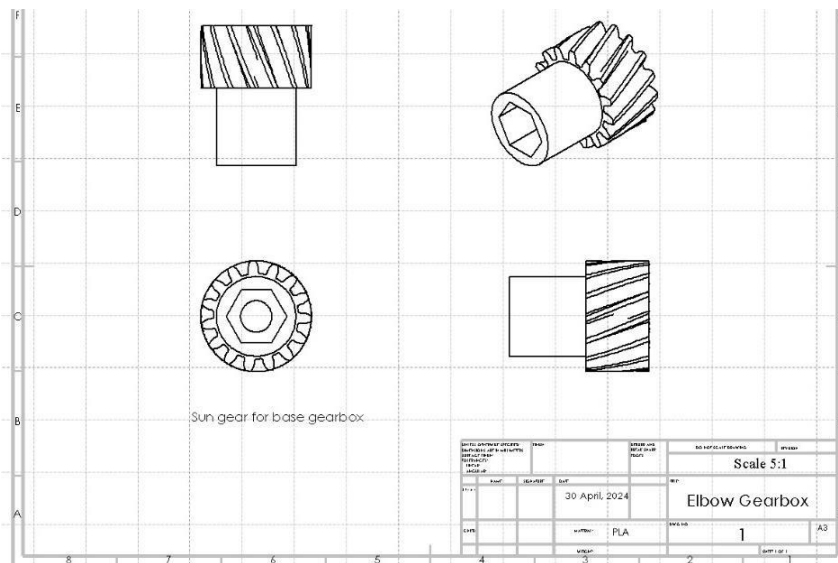**Figure G Shoulder Control Arduino code**
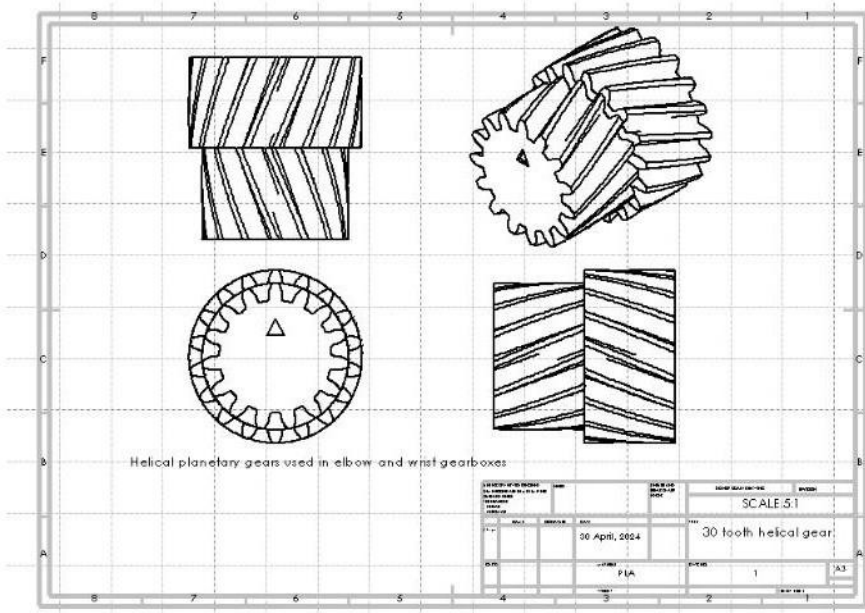

Figure H Arduino motor driving circuit

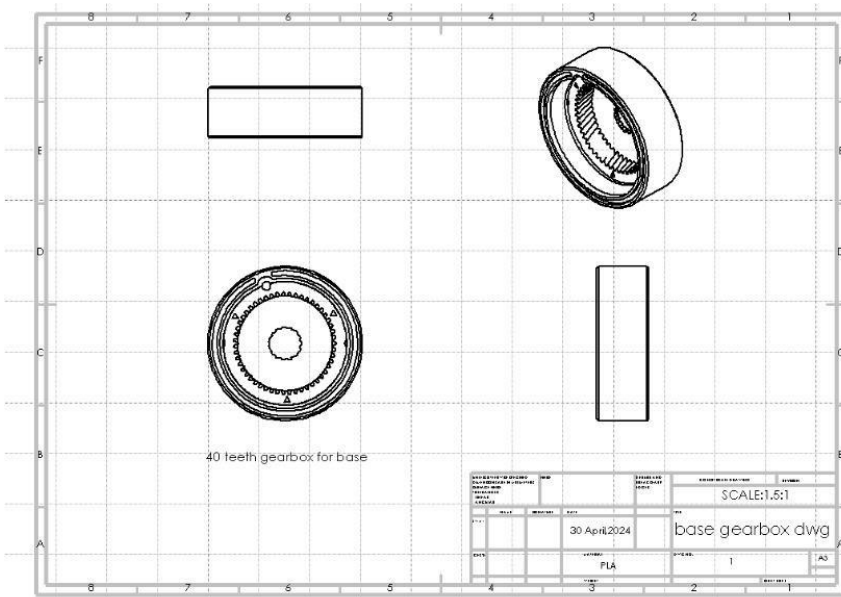**Figure I Connecting plate for Elbow Gearbox**

Figure J Sun gear for Base gearbox

Helical planetary gears used in elbow and wrist gearboxes

SCALE:5:1

30 tooth helical gear

30 April, 2024

PLA

A3

Figure K Planet gear for Elbow gearbox

40 teeth gearbox for base

SCALE:1.5:1

base gearbox dwg

30 April 2024

PLA

A3

Figure L 40 teeth gear for base gearbox

Ring used in base gearbox

Scale 2:1

30 April, 2024

Ring for 40 teeth gears
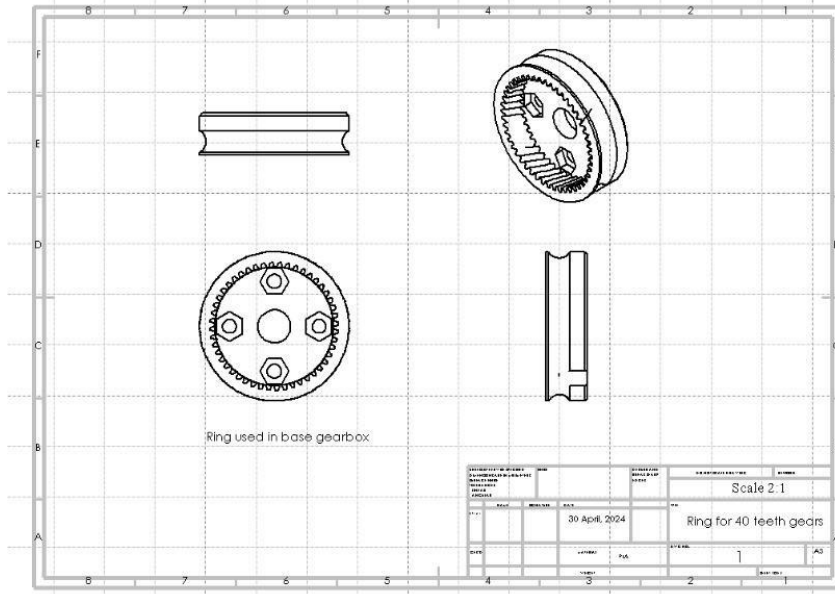
Figure M Ring gear for base gearbox

30 helical teeth elbow gearbox

Scale 1.5:1

30 April, 2024

Elbow Gearbox

PLA
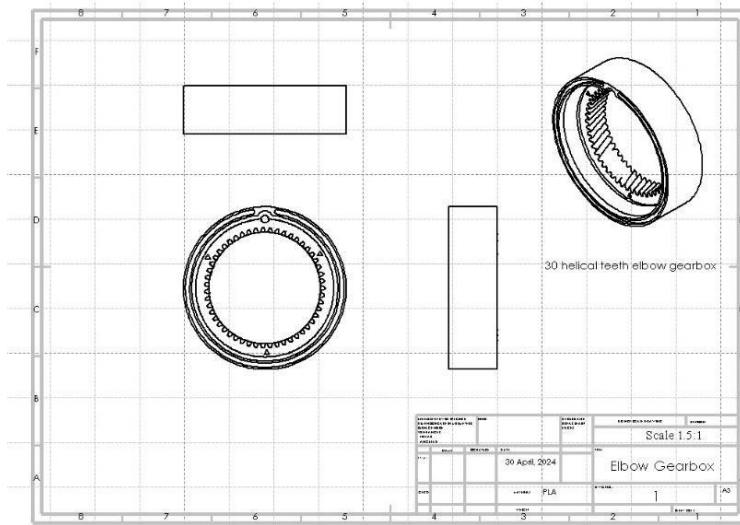
Figure N Ring gear for Elbow gearbox

Sun gear used in elbow and wrist gearboxes

Scale 5:1

00 April, 2024

Sun gear 30 teeth

PLA
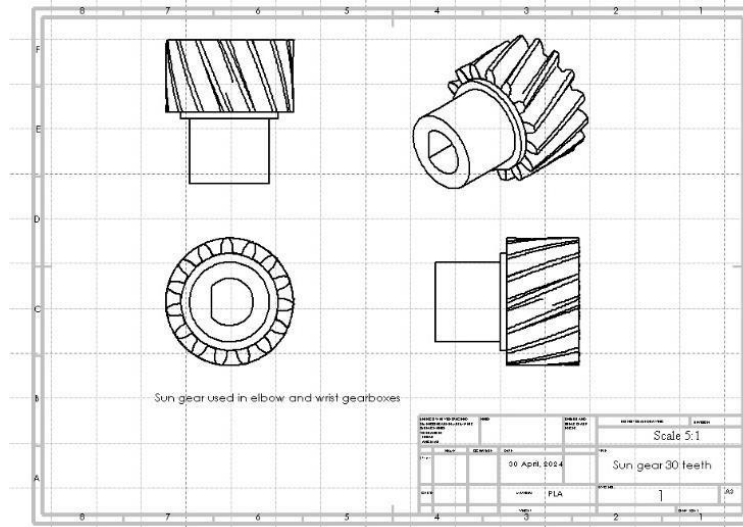
Figure O Sun gear for Elbow gearbox

Helical planetary gears used in base gearbox

Scale 5:1
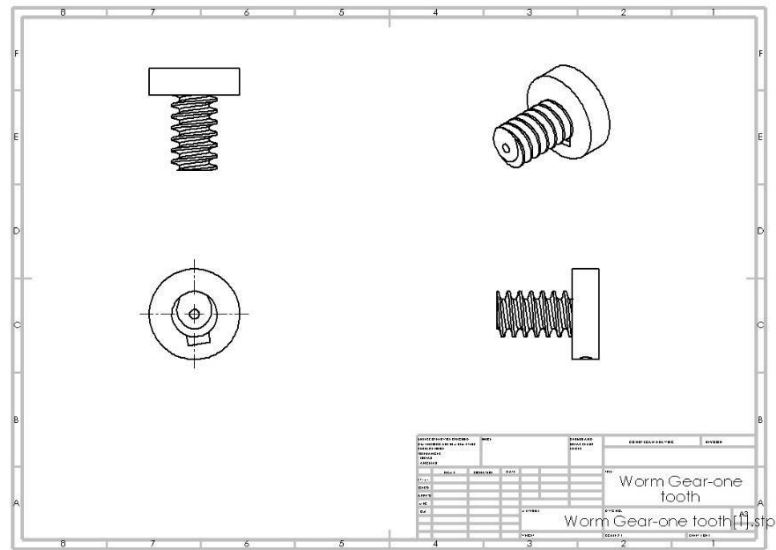
30 April, 2024

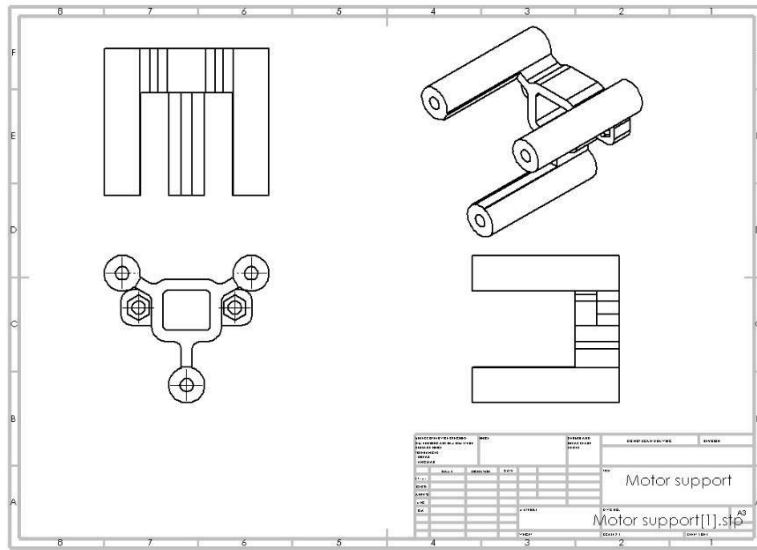helical planetary gear
for base

PLA
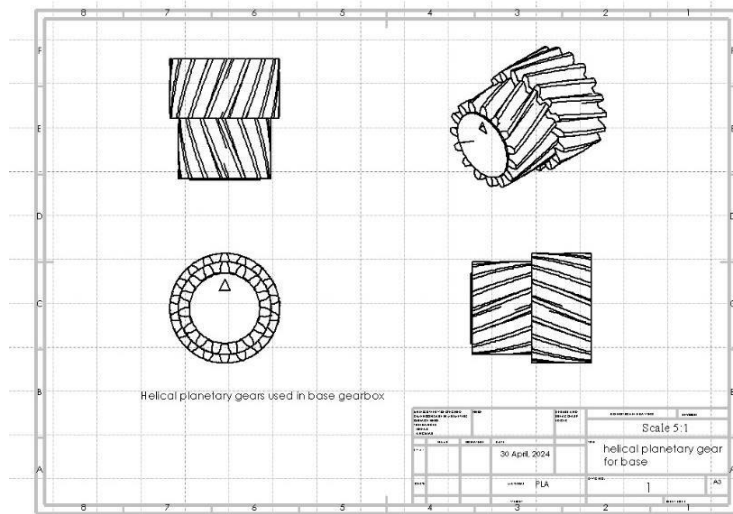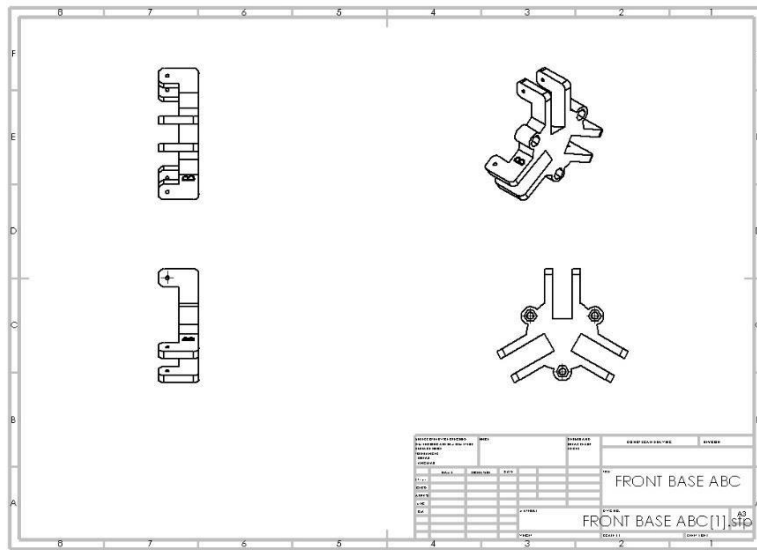
Figure P Planet gear for Base gearbox
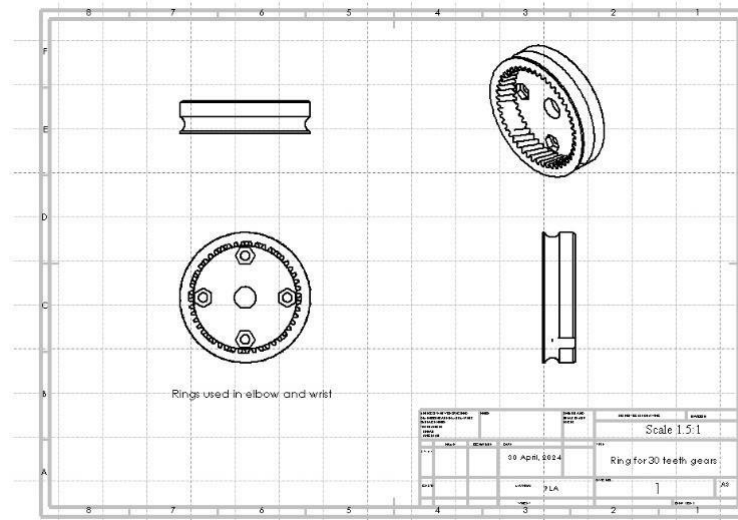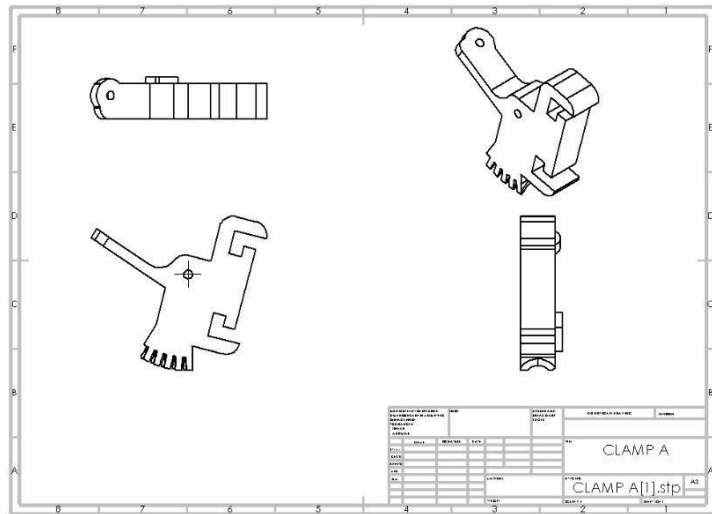
Figure Q Ring gear for Elbow Gearbox

Figure R Lead Screw for Worm Gear
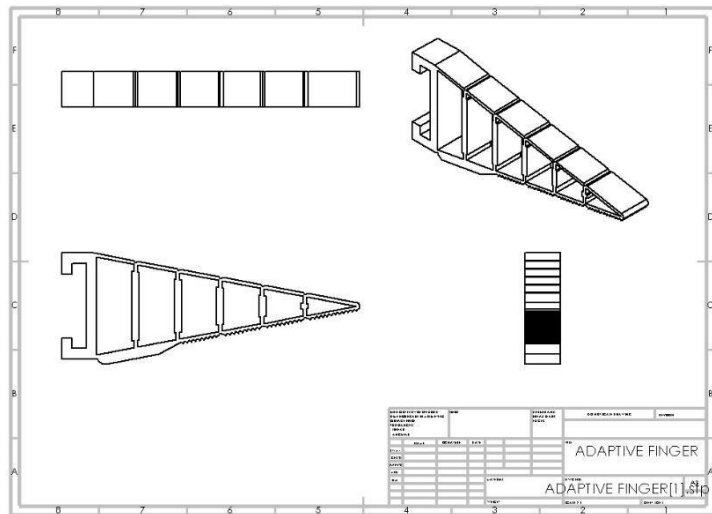
Figure S Motor Support

Figure T Base for Adaptive gripper

Figure U Gripper clamps

Figure V Adaptive Fin Grippers

Table 5 Bill of materials

Gripper	
Parts	Quantity
1.6mm OD x 19mm long nail	8
4G x 9mm long self tapping screw	18
M3 x 25mm long screw	6
M3 x 16mm long screw	12
M3 x 12mm long screw	3
3D Printed Components (PLA)	Multiple
3D Printed Adaptive Finger (TPU)	3
Silicone rubber (20 shore A) or Silicon Chaulk	1
Body	
Parts	Quantity
Countersunk screw M3 x 6mm	18
M4 Nut + screw	18
6mm Steel balls for bearing purpose	50
Cylinder head screw M3 x 9mm + washer	12
Clinder head screw M4 x 7.5mm	8
Clinder head screw M4 x 12mm	8
Cylinder head screw M3 x 10mm + washer	18
4mm and 7 mm drills	1
Clinder head screw M4 x 10mm	8
M3 Nut + screw	12
Countersunk screw M3 x 10mm	12
Cylinder head screw M2.5 x 10mm + washer	8
Cylinder head screw M2.5 x 6mm	16
Countersunk screw M3 x 8mm + washer	16
3D printed components (PLA)	Multiple

Electronics	
Parts	Quantity
Stepper Motors	3
N20 Geared DC motor	1
DRV8825 Motor Driver	3
Arduino Nano	2
Arduino Uno	1
Jumper Wires (Pin to Hole)	50
Jumper Wires (Hole to Hole)	50
Jumper Wires (Pin to Pin)	50
L298N Motor Driver	1
Capacitor	1
Breadboard	3
12 Volts Power Supply	1
Digital Multimeter	1
Myoband	1